

ACCURATE SEGMENTATION OF SYNAPTIC CLEFT WITH CONTOUR GROWING CONCATENATED WITH A CONVNET

Shaobo Min, Xuejin Chen, Hongtao Xie, Zheng-Jun Zha, Guoqiang Bi, Feng Wu, Yongdong Zhang

National Engineering Laboratory for Brain-inspired Intelligence Technology and Application,
University of Science and Technology of China, Hefei, Anhui, China

ABSTRACT

Synaptic cleft is an important area for neuroscientists to analyze the macromolecular complexes related to neurotransmitter transmission. However, the large amount of noise and low signal-to-noise ratio in raw electron micrographs make it challenging to extract this region automatically. In this paper, we propose a simple but effective framework to automatically extract accurate boundaries of synaptic cleft regions. Our approach concatenates a novel contour growing algorithm to a fully convolutional network (FCN), so that it takes both advantages of large receptive field of FCNs and fine-level localization of contour evolution. The contour growing algorithm is based on the flexible evolving tension and synchronous growing controlling to localize the opening contour of cleft region. With consideration of both global localization and local segmentation, our approach is more robust to noisy electron micrographs and outperforms all existing single-model FCNs on accurate segmentation of synaptic clefts.

Index Terms— Synaptic cleft, fully convolutional networks, active contours, contour growing, segmentation

1. INTRODUCTION

Electron micrographs (Fig. 1 (a)) are obtained by cryo-electron tomography (CET) [1, 2], which can visualize the native environment of neurons [3]. Among several studies on CET data [4, 5], synaptic cleft regions are one of the hottest study areas [6], as they play an important role in neurotransmission. In this paper, we propose an automatic approach to accurately extract synaptic cleft regions from noisy electron micrographs (Fig. 1 (b)).

Automatic segmentation of synaptic cleft is challenging in many aspects. Firstly, the synaptic cleft region is typically a quite small fraction of a high-resolution 2D electron micrograph, which requires a high precision of segmenting small objects. Secondly, only the cellular cleft adjacent to one synapse and receiving neurotransmitter molecules from another synapse is the desired synaptic cleft. This requires the segmentation technique to encode more global biological knowledge for judgement. Thirdly, as the most of concerned macromolecules exist on the surface of presynaptic

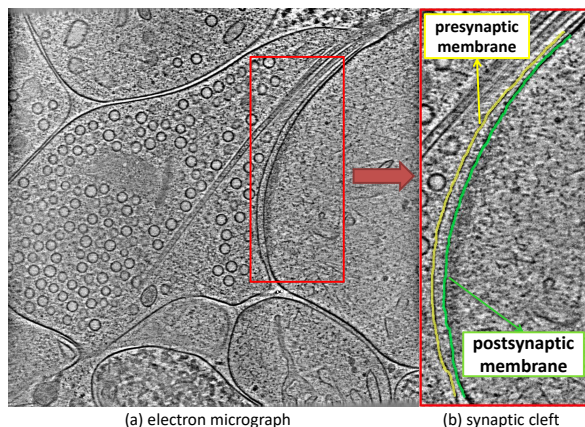


Fig. 1. (a) A synaptic cleft region is indicated by red rectangle in the electron micrograph. (b) The yellow and green curves are respectively the presynaptic and postsynaptic membranes, which are exactly the contours of the cleft region.

membranes, it puts forward a high demand on accurate contour localization.

Active contour was first introduced by Kass et al. [7], which is a popular tools in contour-based segmentation. Cohen et al. [8] added a constant balloon force to drive the curve away from flat regions. Xu et al. [9] proposed a gradient vector flows method for a larger caption field. Later, open active contour models have been proposed for medical image analysis to extract tree-shaped structures [10] by evolving and growing. These methods require a good contour initialization and a clean image quality, both of which are unsatisfied in electron micrographs. Recently, fully convolutional networks (FCN) and deep learning [11, 12, 13, 14, 15, 16] have made a significant progress in image segmentation. The famous U-net [17] utilized the skip-connection to retain more details. Chen et al. [18] proposed a dilated convolution to enlarge the receptive fields for fewer pooling operations. Moreover, PSP-Net [19] uses the powerful ResNet [20] and a pyramid pooling module to extract better context features. However due to successive downsampling layers, FCN based methods fail to give accurate contour localization in this segmentation task.

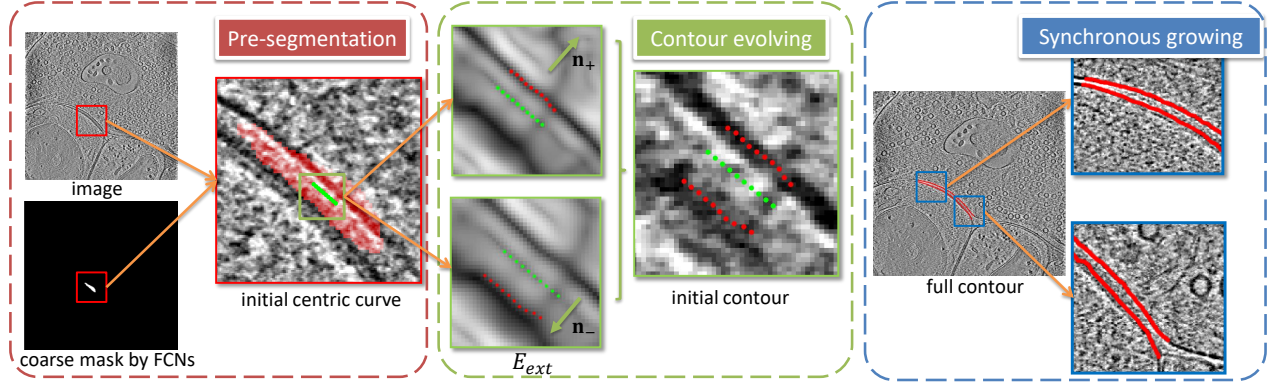


Fig. 2. A brief view of our algorithm. First, a FCN-style network provides a coarse segmentation mask, which gives an initial curve (green line) for next evolving. Then, the initial curve is respectively evolved along opposite directions to attach to both membranes. Finally, two curves synchronously grow to localize the whole synaptic cleft region (encircled by red solid curves).

In this paper, we propose an segmenting framework for electron micrographs by combining intelligent FCNs and a novel contour growing algorithm. Our method consists of two steps. First, a FCN-based segmentation is employed to coarsely segment the synaptic cleft region. Then, our proposed contour growing algorithm will result in precise contour localizations of target synaptic cleft region with previous coarse segmentation.

Especially, our contour growing method is a self-correcting model, consisting of contour evolving and synchronously growing algorithms. With a coarse segmentation of the target region, we first generate an initial centric curve and then evolve it twice to attach to two synaptic membranes using our contour evolving algorithm. Different from GVF [9], we propose a novel updating strategy that is more robust to image noise. Finally a synchronously growing algorithm is developed to gradually grow both curves to encircle the entire target region. Especially, the growing of both curves are synchronous, and terminates according to the distance between the two membranes. The whole framework is shown in Fig. 2 In summary, our main contribution is twofold: 1) We propose an effective framework to accurately segment synaptic cleft regions in electron micrographs; 2) A novel updating strategy of active contours is developed, which is more robust and effective for accurate extraction of synaptic cleft regions.

2. PROPOSED ALGORITHM

The pipeline of our algorithm is shown in Fig. 2, which contains three steps: a) pre-segmentation by FCNs; b) contour evolving based on initial curves; c) synchronous growing.

2.1. FCN segmentation

In Fig. 2, we obtain the coarse mask using the DeepLab variant (ResNet-101), whose classifier is modified to a binary

classifier and loss function is weighted for mitigating the unbalanced label problem. Then, an centric curve is generated from the coarse mask as the initial curves of the following steps. Explicitly, the initial curve is obtained by fitting a quadratic spline on all the positive pixels in the mask and truncating the middle part in a small length ,such as the green dotted line in Fig. 2.

2.2. Curve evolving

Similar to the traditional snake model [7], the initial curve is expressed by a parameterized model $\mathbf{v}(s) = (x(s), y(s))$, where $s \in [0, 1]$ is the arc-length along the curve. Our goal is to minimize the following energy function:

$$\begin{aligned} E_{total} &= \int_0^1 E_{int}(\mathbf{v}(s)) + E_{ext}(\mathbf{v}(s)) ds & (1) \\ E_{int} &= \alpha |\mathbf{v}'(s)|^2 + \beta |\mathbf{v}''(s)|^2 \\ E_{ext} &= I(\mathbf{v}(s)) + \kappa G(\mathbf{v}(s)), \end{aligned}$$

where $\mathbf{v}'(s)$ and $\mathbf{v}''(s)$ are the derivatives of $\mathbf{v}(s)$, controlling the curve to be smooth. G is the gradient magnitude map, which drives the curve to the edge region. According to [7], Eq. (1) can be minimized by iteratively updating the equation:

$$\begin{aligned} \mathbf{x}_{t+1} &= (\mathbf{A} + \gamma \mathbf{I})^{-1} (\mathbf{x}_t - \mathbf{f}_x(\mathbf{x}_t, \mathbf{y}_t)) & (2) \\ \mathbf{y}_{t+1} &= (\mathbf{A} + \gamma \mathbf{I})^{-1} (\mathbf{y}_t - \mathbf{f}_y(\mathbf{x}_t, \mathbf{y}_t)), \end{aligned}$$

where $\mathbf{x}, \mathbf{y} \in R^{n_p}$ are coordinates of n_p controlling points. \mathbf{A} is a pentadiagonal banded matrix [7], γ is a step size and $\mathbf{f}_x, \mathbf{f}_y$ are the gradient maps calculated from E_{ext} using Gradient Vector Flow (GVF) algorithm [9].

As we know, $\mathbf{f}(\mathbf{x}_t, \mathbf{y}_t)$ is sensitive to image noise. Thus gradient guided evolving is improper in our electron micrographs with high noise. For example in flat regions, the gradients are too weak for efficiently evolving, which puts higher

demand on initial curves. And in noise region, the gyrate tension caused by noisy gradients easily trap the control points. Thus in this section, we propose a new updating strategy by:

$$\begin{aligned} \mathbf{x}_{t+1} &= (\mathbf{A} + \gamma \mathbf{I})^{-1}(\mathbf{x}_t + E_{ext}(\mathbf{x}_t, \mathbf{y}_t) \mathbf{n}_x) \\ \mathbf{y}_{t+1} &= (\mathbf{A} + \gamma \mathbf{I})^{-1}(\mathbf{y}_t + E_{ext}(\mathbf{x}_t, \mathbf{y}_t) \mathbf{n}_y), \end{aligned} \quad (3)$$

where $\mathbf{n}_x, \mathbf{n}_y \in R^{n_p}$ make up the normal vectors of n_p controlling points with consistent orientations.

In Eq. (3), the direction of external tension is fixed as the normal direction of each controlling point, whose magnitude is E_{ext} rather than a constant value in Ballons model [8]. The advantages of Eq. (3) are as follows: a) the capture range of external tension is much larger, due to fixed external tension along normal direction; b) the external tension in noisy regions is no longer gyrate. c) our external tension will soon vanish in contour region due to small E_{ext} , which makes the updating more robust. By setting two opposite normal vectors (\mathbf{n}_+ and \mathbf{n}_- in Fig. 2), the centric curve will be evolved along two opposite directions and well attach to the presynaptic and postsynaptic membranes. The final evolved curves are respectively denoted as $\mathbf{c}_1(s)$ and $\mathbf{c}_2(s)$.

2.3. Synchronous growing

With the two initial pieces of contour $\mathbf{c}_1(s)$ and $\mathbf{c}_2(s)$, we then grow them to localize the whole cleft region. The challenge of this part is that they should be grown correctly and synchronously to compute the exact distance between two membranes for termination judging.

First, we formulate the process of growing a contour $\mathbf{c}(s)$ as iteratively finding a piece of straight line segment with length l and unit vector \mathbf{v}_l :

$$\arg \min_{l, \mathbf{v}_l} \frac{1}{l} \sum_{i=0}^l E_{ext}(i \mathbf{v}_l + \mathbf{q}) - \rho \mathbf{v}_q \cdot \mathbf{v}_l, \quad (4)$$

st. $\mathbf{v}_q \cdot \mathbf{v}_l > \tau$.

where \mathbf{q} is the current endpoint of $\mathbf{c}(s)$, and \mathbf{v}_q is the tangent vector of \mathbf{q} on the curve. Similarly, we use l points to represent the target straight line length for convenience. The first term of Eq. (4) expects $\mathbf{c}(s)$ to grow along the membranes with small E_{ext} , while the second term prefers the growing direction following the previous direction of the contour. ρ is a tradeoff parameter, and τ adds a hard constraint on the growing direction to be not changed too much. Optimal solution of Eq. (4) can be obtained by alternatively updating l and \mathbf{v}_l . First, we fix l as a small value (5 pixels) to find an optimal \mathbf{v}_l , and then fix \mathbf{v}_l to find a better l . Experiments show that two iterations are good enough for most cases to generate a satisfying piece of new growing membrane.

To synchronously grow $\mathbf{c}_1(s)$ and $\mathbf{c}_2(s)$, we split the growing process into several periods and decide which curve grows in each period. Especially, we set two variables g_1^{t+1}

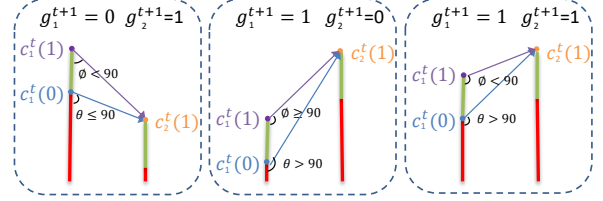


Fig. 3. Different situations of Eq. (5). The green lines are new growing contours, and the red lines are previous contours.

and g_2^{t+1} (1 for growing and 0 for waiting) to determine the growing state of $\mathbf{c}_1^t(s)$ and $\mathbf{c}_2^t(s)$ at stage $t + 1$ by:

$$g_1^{t+1}, g_2^{t+1} = \begin{cases} 0, 1 & \text{if } \phi \leq 90^\circ \text{ and } \theta \leq 90^\circ \\ 1, 0 & \text{if } \phi > 90^\circ \text{ and } \theta > 90^\circ \\ 1, 1 & \text{else.} \end{cases} \quad (5)$$

Different situations of Eq. (5) are shown in Fig. 3. The distance between two membranes is calculated by:

$$d^t = \frac{\|\mathbf{q}^t - \mathbf{p}^t\| + \|\mathbf{q}^{t-1} - \mathbf{p}^{t-1}\|}{2}, \quad (6)$$

where \mathbf{q}^t and \mathbf{p}^t are the endpoints of two membranes. Once d^t is beyond the a reasonable cleft width, the growth stops.

3. EXPERIMENTS

Dataset. Synaptic images are obtained by cryo-electron tomography (CET), from which we can directly observe a native environment of synaptic structures in a high resolution (about 1500×1500). In this paper, our goal is to extract the synaptic cleft region, which is adjacent to a synapse and receives neurotransmitter molecules from another synapse. And only the cleft between two synapses, whose width is about $20 \sim 30$ nm ($20 \sim 70$ pixels in our electron micrographs), might be the desired synaptic cleft. We build a dataset of synaptic electron micrographs, including 400 synaptic images for training and 159 images for testing. All the image are observed in the raw resolution and labeled by experts.

Implementation details. The training strategy of our DeepLab module follows the original paper [18]. For such a high resolution of electron micrographs, we crop 321×321 patch from original image as the input to DeepLab. In order to avoid overfitting, we fine-tune the weights of lower layers on the off-the-shelf model, which has been well trained on natural images. The data augmentation, including rotations and flipings in [18] is also applied. During the contour evolving, α , β , κ in Eq. (1) and γ in Eq. (3) are respectively set as 0.2, 0.2, 0.3 and 1, which can give the best performance in our dataset. For synchronous growing, $\rho = 2.5$ and $\tau = \frac{\sqrt{2}}{2}$ in Eq. (4) to constrain the growing direction deviating $[-\frac{\pi}{4}, \frac{\pi}{4}]$ from the previous growing direction. When d^t in Eq. (6) is beyond the range of $[20, 90]$, the growth is terminated.

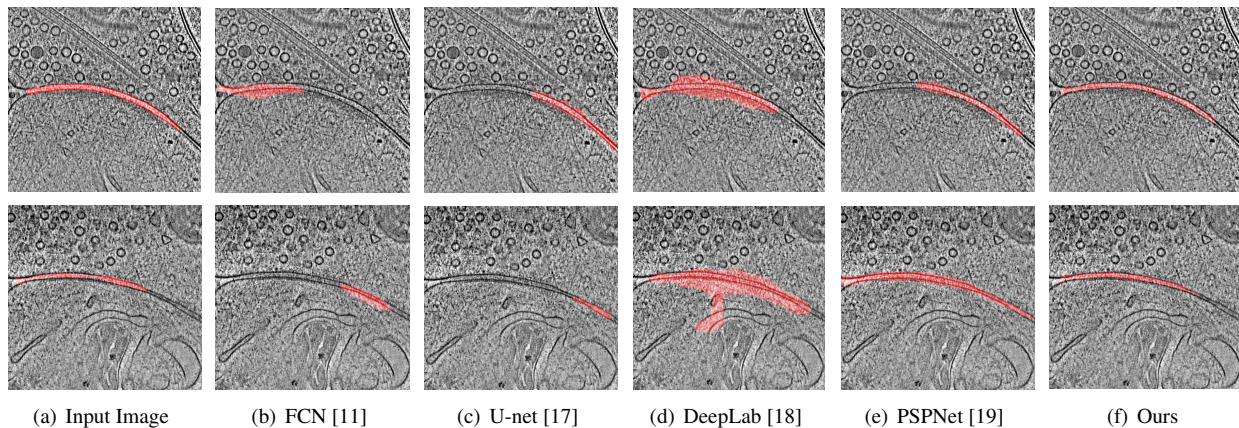


Fig. 4. Results produced by state-of-the-art segmentations methods and our model. The red regions in input images are the ground truth, while the others are predicted target regions.

Table 1. Results of comparing with state-of-the-art methods.

Methods	Pixel Accu.	mean IOU
FCN [11]	0.9923	0.5258
U-net [17]	0.9939	0.6359
DeepLab [18]	0.9951	0.7164
PSPNet [19]	0.9949	0.7195
FCN+GVF	0.9724	0.6145
FCN+balloon	0.9794	0.6345
FCN+CG (ours)	0.9974	0.7848

Table 2. Contour growing with various pre-segmentations.

Methods	Pixel Accu.	mean IOU
Contour Growing+FCN	0.9956	0.6339
Contour Growing+U-net	0.9962	0.7720
Contour Growing+DeepLab	0.9974	0.7848
Contour Growing+PSPNet	0.9961	0.7683

Evaluation metrics. We use two metrics to evaluate our method on the segmentation task: a) pixel accuracy, which evaluates the percentage of true predicted pixels over the whole pixels; b) pixel intersection-over-union (IOU) averaged across different classes (two labels in our task).

Results We compare our algorithm with several state-of-the-art methods, including FCN [11], U-net [17], DeepLab [18] and PSPNet [19]. Especially, DeepLab indicates the ResNet101 version of [18]. Furthermore, we also compare our evolving model with Eq.(3) to the GVF [9] and balloon model [8].

Table 1 reports the pixel accuracy and mean IOU of different methods. Our method outperforms any single FCN. The common high pixel accuracy is caused by extreme unbalanced labels, most of which are background. Fig. 4 compares the cropped segmentation results of different methods, which shows that our localized contours are much more precise and complete. It can be also observed that FCNs can localize the

correct positions of synaptic cleft in most cases, but their contours are not precise enough for further analysis. More results with the raw-resolution are provided in supplementary materials. Especially, U-net performs better than FCN, due to richer features extracted by the U-shaped architecture. And pyramid pooling module in PSPNet really benefits the contour localization. Finally compared with GVF, our superior results indicates that the proposed updating strategy performs better than GVF and balloon model in handling such noisy images.

In order to further demonstrate the robustness of our approach to different initial segmentation, we explore the effects of various pre-segmentation modules on our contour growing results. From the results in Table 2, it demonstrates that our contour growing algorithm can obviously improve the results of different pre-segmentation models. And more visual results are provided in the supplementary material.

4. CONCLUSION

In this paper, a segmentation method is proposed for synaptic cleft in cryo-electron tomography. With the initial curve from FCN, a contour growing algorithm is developed to localize the accurate contours by evolving and growing. Instead of GVF, a novel updating strategy for contour evolving is proposed which is more robust to image noise. Our future work will connect FCN and contour growing as an end-to-end framework, which may benefits both of them.

5. ACKNOWLEDGEMENT

This work was supported by the National Natural Science Foundation of China under Grant 61632006, 61622211, 61620106009 and 61525206, the Fundamental Research Funds for the Central Universities (No. WK2380000002, WK3490000003, and WK2100100030).

6. REFERENCES

- [1] Benoît Zuber, Irina Nikonenko, Paul Klauser, Dominique Muller, and Jacques Dubochet, “The mammalian central nervous synaptic cleft contains a high density of periodically organized complexes,” *Proceedings of the National Academy of Sciences*, vol. 102, no. 52, pp. 19192–19197, 2005.
- [2] Peter W Hawkes, “The electron microscope as a structure projector,” in *Electron tomography*, pp. 83–111. Springer, 2007.
- [3] Vladan Lučić, Friedrich Förster, and Wolfgang Baumeister, “Structural studies by electron tomography: from cells to molecules,” *Annu. Rev. Biochem.*, vol. 74, pp. 833–865, 2005.
- [4] Martin Beck, Vladan Lučić, Friedrich Förster, Wolfgang Baumeister, and Ohad Medalia, “Snapshots of nuclear pore complexes in action captured by cryo-electron tomography,” *Nature*, vol. 449, no. 7162, pp. 611, 2007.
- [5] Vladan Lučić, Alexander Rigort, and Wolfgang Baumeister, “Cryo-electron tomography: the challenge of doing structural biology in situ,” *J Cell Biol.*, vol. 202, no. 3, pp. 407–419, 2013.
- [6] Hajime Hirasawa and Akimichi Kaneko, “ph changes in the invaginating synaptic cleft mediate feedback from horizontal cells to cone photoreceptors by modulating ca²⁺ channels,” *The Journal of general physiology*, vol. 122, no. 6, pp. 657–671, 2003.
- [7] Michael Kass, Andrew Witkin, and Demetri Terzopoulos, “Snakes: Active contour models,” *International journal of computer vision*, vol. 1, no. 4, pp. 321–331, 1988.
- [8] Laurent D Cohen, “On active contour models and balloons,” *CVGIP: Image understanding*, vol. 53, no. 2, pp. 211–218, 1991.
- [9] Chenyang Xu and Jerry L Prince, “Snakes, shapes, and gradient vector flow,” *IEEE Trans. on image processing*, vol. 7, no. 3, pp. 359–369, 1998.
- [10] T. Xu, H. Li, T. Shen, N Ojkic, D Vavylonis, and X. Huang, “Extraction and analysis of actin networks based on open active contour models,” *Proc. IEEE Int. Symp. Biomed. Imaging*, pp. 1334–1340, 2011.
- [11] Jonathan Long, Evan Shelhamer, and Trevor Darrell, “Fully convolutional networks for semantic segmentation,” in *Proceedings of the IEEE Conference on CVPR*, 2015, pp. 3431–3440.
- [12] Chang Chen, Xinmei Tian, Zhiwei Xiong, and Feng Wu, “Udnet: Up-down network for compact and efficient feature representation in image super-resolution,” in *The IEEE International Conference on Computer Vision (ICCV) Workshops*, Oct 2017.
- [13] Chang Chen, Zhiwei Xiong, Xinmei Tian, and Feng Wu, “Deep boosting for image denoising,” in *ECCV*, 2018.
- [14] Xin Miao, Xiantong Zhen, Xianglong Liu, Cheng Deng, Vassilis Athitsos, and Heng Huang, “Direct shape regression networks for end-to-end face alignment,” in *The IEEE Conference on Computer Vision and Pattern Recognition (CVPR)*, June 2018.
- [15] Chaojie Wang, Bo Chen, and Mingyuan Zhou, “Multi-modal poisson gamma belief network,” in *Thirty-Second AAAI Conference on Artificial Intelligence*, 2018.
- [16] Bin Gu, Miao Xin, Zhouyuan Huo, and Heng Huang, “Asynchronous doubly stochastic sparse kernel learning,” in *Thirty-Second AAAI Conference on Artificial Intelligence*, 2018.
- [17] Olaf Ronneberger, Philipp Fischer, and Thomas Brox, “U-net: Convolutional networks for biomedical image segmentation,” in *International Conference on Medical Image Computing and Computer-Assisted Intervention*. Springer, 2015, pp. 234–241.
- [18] LC Chen, G Papandreou, I Kokkinos, K Murphy, and AL Yuille, “DeepLab: Semantic image segmentation with deep convolutional nets,” *Atrous Convolution, and Fully Connected CRFs. arXiv*, 2016.
- [19] Hengshuang Zhao, Jianping Shi, Xiaojuan Qi, Xiaogang Wang, and Jiaya Jia, “Pyramid scene parsing network,” *arXiv preprint arXiv:1612.01105*, 2016.
- [20] Kaiming He, Xiangyu Zhang, Shaoqing Ren, and Jian Sun, “Deep residual learning for image recognition,” in *Proceedings of the IEEE conference on computer vision and pattern recognition*, 2016, pp. 770–778.